

Bright solitary waves in a Bose-Einstein condensate and their interactions

K. Kärkkäinen¹, A. D. Jackson² and G. M. Kavoulakis³

¹*Mathematical Physics, Lund Institute of Technology, P.O. Box 118, SE-22100 Lund, Sweden*

²*Niels Bohr Institute, Blegdamsvej 17, DK-2100, Copenhagen Ø, Denmark*

³*Technological Education Institute of Crete, P.O. Box 1939, GR-71004, Heraklion, Greece*

(Dated: November 21, 2018)

We examine the dynamics of two bright solitary waves with a negative nonlinear term. The observed repulsion between two solitary waves – when these are in an antisymmetric combination – is attributed to conservation laws. Slight breaking of parity, in combination with weak relaxation of energy, leads the two solitary waves to merge. The effective repulsion between solitary waves requires certain nearly ideal conditions and is thus fragile.

PACS numbers: 03.75.-b, 03.75.Lm

I. INTRODUCTION

One of the many interesting features of Bose-Einstein condensed atoms is that they can support solitary waves, in particular when these are confined in elongated traps. Under typical conditions, these gases are very dilute and are described by the familiar Gross-Pitaevskii equation, a nonlinear Schrödinger equation with an additional term to describe the external trapping potential.

It is well known that the nonlinear Schrödinger equation (with no external potential) supports solitonic solutions through the interplay between the nonlinear term and dispersion. In the presence of an external trapping potential, the Gross-Pitaevskii equation becomes non-integrable. In elongated quasi-one-dimensional traps, it is reasonable to approximate the three-dimensional solution of the Gross-Pitaevskii equation by separating longitudinal and transverse degrees of freedom [1]. The resulting effective one-dimensional nonlinear equation has a nonlinear term that is not necessarily quadratic [1, 2]. Still, such nonlinear equations support solitary-wave solutions, which must be found numerically.

Solitary waves have been created and observed in trapped gases of atoms [3, 4, 5, 6]. In the initial experiments [3, 4] the effective interaction between the atoms was repulsive. In this case, the solitary waves are localized depressions in the density, which are known as “grey” solitary waves. These waves move with a velocity less than the speed of sound. When the minimum of the density (at the center of the wave) becomes zero, they do not move at all and thus become “dark”.

More recently, the two experiments of Refs. [5, 6] considered the case of an effective attraction between the atoms and observed “bright” solitary waves, i.e., blob(s) of atoms which preserve their shape and distinct identity. Strecker *et al.* [5] created an initial state of many separate solitary waves. While these independent waves were seen to oscillate in the weak harmonic potential in the longitudinal direction, they did not merge to form one solitary wave. In other words, they behaved as if the effective interaction between two of these waves were repulsive.

Numerous theoretical studies have been motivated by

the experiments of Refs. [5, 6], see e.g., Refs. [7, 8, 9]. Reference [7] offered an explanation for the observed effective repulsion between solitary waves. As argued there, the experiments had been performed in a manner that gave rise to a phase difference of π between adjacent solitary waves. According to an older study [10], solitary waves with a phase difference equal to π indeed repel each other.

In the present study we use a toroidal trap [11] as a model for examining the time evolution of a system that initially has two solitary waves using numerical solutions to the corresponding time-dependent one-dimensional Gross-Pitaevskii equation. Remarkably, such toroidal traps have been designed [12], and very recently persistent currents have been created and observed in such traps [13]. The basic conclusion of our study is that the effective repulsion between solitary waves is due to conservation laws and thus fragile.

In what follows, we first present our model in Sec II. In Sec. III we examine the dynamics of the gas in the case of weak dissipation, starting with perfectly symmetric/antisymmetric initial conditions and with no external potential along the torus. We observe that the symmetric configuration of two blobs merges on a short time scale; the blobs in the initially antisymmetric configuration remain distinct and separated. Using these results as “reference” plots, we examine in Sec. IV the effect of a weak random potential on perfectly symmetric/antisymmetric initial conditions. We also examine in Sec. V the time evolution of states that deviate slightly from perfect symmetry/antisymmetry in the absence of any random potential. In both cases, the symmetric (or nearly symmetric) initial configuration shows essentially the same behavior as the reference symmetric system. On the other hand, the antisymmetric configuration with the addition of an extra weak random potential and the nearly antisymmetric configuration with no external potential both lead to a merger of the two blobs after a moderate transient time. In the antisymmetric case, the final state is strongly influenced by weak deviations from the “ideal” case. Finally, in Sec. VI we discuss our results.

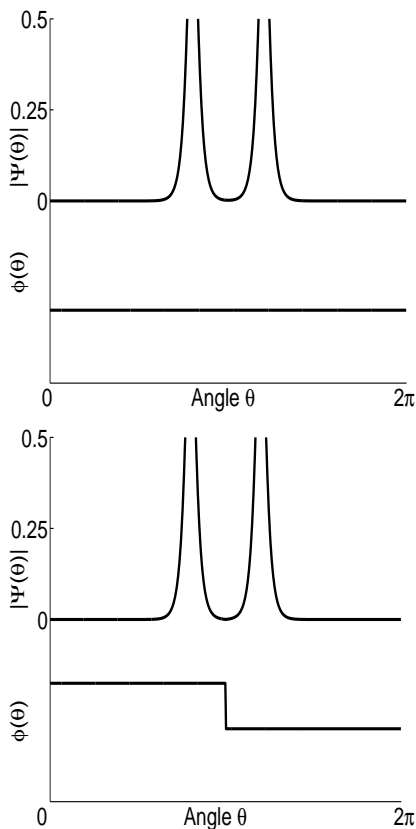


FIG. 1: Plot of $|\Psi(\theta, t = 0)|$ and of $\phi(\theta, t = 0)$ for the symmetric (higher) and for the antisymmetric (lower) case, $\alpha = \pm 1$ in Eq. (3).

II. MODEL

We consider a tight toroidal trap and use the mean-field approximation. Tight confinement along the cross section of the torus allows us to assume that the transverse degrees of freedom are frozen, and thus the corresponding time-dependent order parameter $\Psi(\theta, t)$ satisfies the (one-dimensional) equation

$$i\hbar \frac{\partial \Psi}{\partial t} = \frac{\hbar^2}{2MR^2} \left[-\frac{\partial^2 \Psi}{\partial \theta^2} + g|\Psi|^2\Psi + V(\theta)\Psi \right], \quad (1)$$

where $g = 8\pi NaR/S$, and $V(\theta)$ is the external potential measured in units of $E_0 = \hbar^2/(2MR^2)$. Here, M is the atomic mass, R is the radius of the torus, N is the atom number, a is the scattering length (which is taken to be negative), and S is the cross section of the torus. The total length of the torus is chosen to be 16π in our simulations.

As shown in Refs. [14, 15], below a critical (negative) value of the parameter g , there is an instability from a state of homogeneous density to a state with localized density that breaks the rotational invariance of the Hamiltonian. This localized state corresponds to a solitary wave, and the critical value of g is $g_c = -\pi$ for the parameters chosen here. We adopt the value of

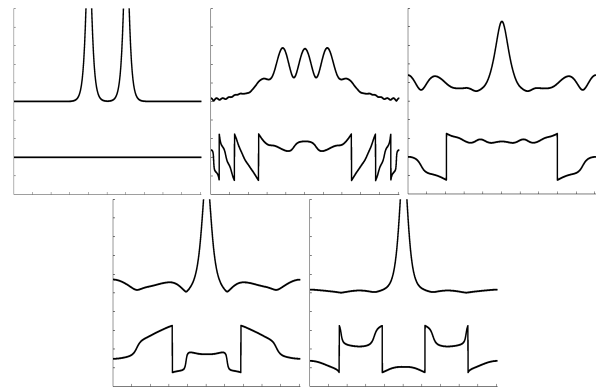


FIG. 2: Snapshots of $|\Psi(\theta, t)|$ (higher curve in each panel) and of $\phi(\theta, t)$ (lower curve in each panel) of the order parameter $\Psi = |\Psi(\theta, t)|e^{i\phi(\theta, t)}$, for the symmetric initial configuration, $\alpha = 1$, for $t/t_0 = 0, 10, 50, 100$, and 150 . The axes are the same as in Fig. 1. In all the above graphs there is no external potential, $V = 0$.

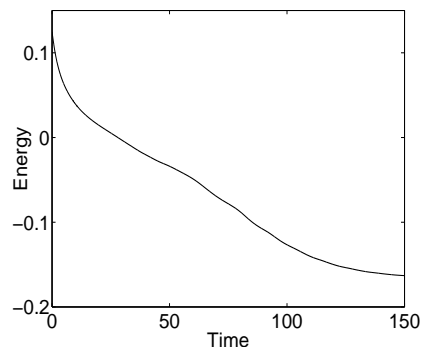


FIG. 3: The energy of the system in units of $E_0 = \hbar^2/(2MR^2)$, versus time for $0 \leq t/t_0 \leq 150$ corresponding to Fig. 2.

$g = -4 < g_c$ in all simulations below. Therefore, the lowest energy state is a single solitary wave.

We add an extra term on the left side of the above equation to model dissipation and write

$$(i - \gamma)\hbar \frac{\partial \Psi}{\partial t} = \frac{\hbar^2}{2MR^2} \left[-\frac{\partial^2 \Psi}{\partial \theta^2} + g|\Psi|^2\Psi + V(\theta)\Psi \right]. \quad (2)$$

The real positive dimensionless parameter γ describes the “strength” of dissipation. Since we solve an initial value problem, we also need to specify the initial condition. This is

$$\Psi(\theta, t = 0) = \frac{1}{\sqrt{1 + \alpha^2}} [\psi(\theta - \theta_0) + \alpha\psi(\theta + \theta_0)]. \quad (3)$$

Here $\psi(\theta) = \lambda/\cosh(\lambda\theta)$, with $\lambda = 3/2$, is a static, well localized blob. We choose $\theta_0 = 2\pi/5$ so that the two blobs are reasonably distinct but still have a small overlap, as shown in the graphs of Fig. 1, for $\alpha = \pm 1$.

Figures 2, 4, 6, 8, 10 and 12 show snapshots of $|\Psi(\theta, t = 0)|$ and of $\phi(\theta, t = 0)$ for the order parameter $\Psi(\theta, t) = |\Psi(\theta, t)|e^{i\phi(\theta, t)}$. Figs. 3, 5, 7, 9, 11, and 13

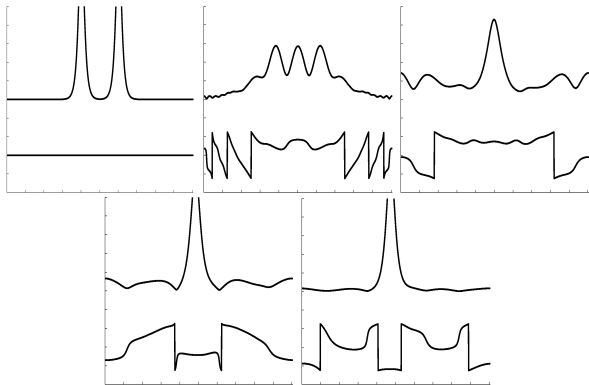


FIG. 4: Snapshots of $|\Psi(\theta, t)|$ (higher curve in each panel) and of $\phi(\theta, t)$ (lower curve in each panel) of the order parameter $\Psi = |\Psi(\theta, t)|e^{i\phi(\theta, t)}$, for the symmetric initial condition, for $t/t_0 = 0, 10, 50, 100$, and 150 , for a weak random potential (shown in Fig. 14), with a symmetric initial configuration, $\alpha = 1$. The axes are the same as in Fig. 1.

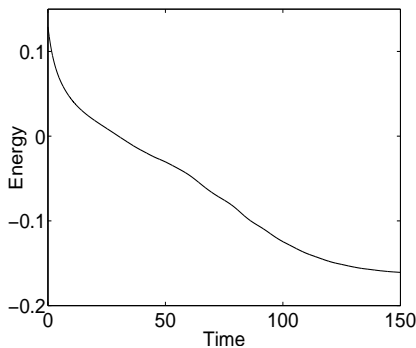


FIG. 5: The energy of the system in units of $E_0 = \hbar^2/(2MR^2)$, versus time for $0 \leq t/t_0 \leq 150$ corresponding to Fig. 4.

show the corresponding energy of the gas as function of time.

III. TIME EVOLUTION OF THE “IDEAL” SITUATION

To understand the effects of a weak random potential and the effect of slight asymmetries in the initial condition (to be considered in Secs. IV and V), it is instructive to start with the situation where there is no external potential, $V(\theta) = 0$ and an initial configuration which is either perfectly symmetric ($\alpha = 1$), or perfectly antisymmetric ($\alpha = -1$), i.e.,

$$\Psi(\theta, t = 0) = \frac{1}{\sqrt{2}}[\psi(\theta - \theta_0) \pm \psi(\theta + \theta_0)]. \quad (4)$$

We also fix the value of the dissipative parameter equal to $\gamma = 0.05$. Figures 2 and 8 show snapshots of $|\Psi(\theta, t)|$ as well as the phase $\phi(\theta, t)$ of the order parameter $\Psi(\theta, t)$ for the symmetric and the antisymmetric

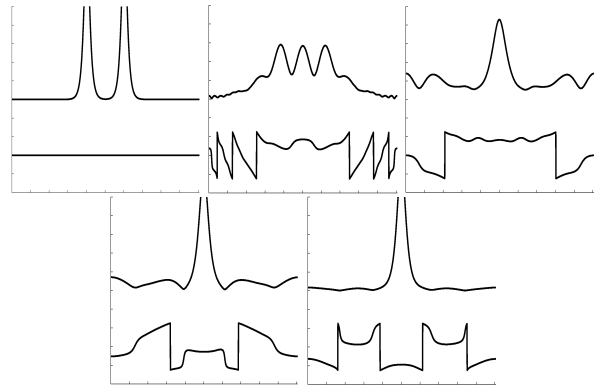


FIG. 6: Snapshots of $|\Psi(\theta, t)|$ (higher curve in each panel) and of $\phi(\theta, t)$ (lower curve in each panel) of the order parameter $\Psi = |\Psi(\theta, t)|e^{i\phi(\theta, t)}$, for the almost symmetric initial condition, $\alpha = 1.01$, for $t/t_0 = 0, 10, 50, 100$, and 150 . The axes are the same as in Fig. 1. In all the above graphs there is no external potential, $V = 0$.

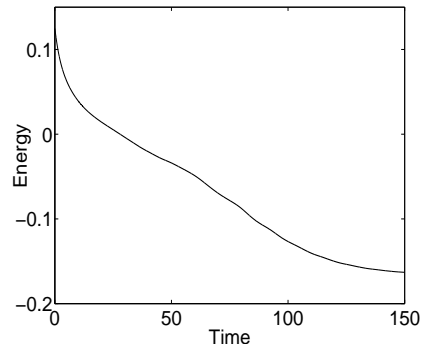


FIG. 7: The energy of the system in units of $E_0 = \hbar^2/(2MR^2)$, versus time for $0 \leq t/t_0 \leq 150$ corresponding to Fig. 6.

case, respectively. The snapshots shown in Fig. 2 correspond to $t/t_0 = 0, 10, 50, 100$, and 150 , and in Fig. 8 to $t/t_0 = 0, 10, 100, 300$, and 400 . Here $t_0 = E_0/\hbar = [\hbar/(2MR^2)]^{-1}$ is the unit of time. Figures 3 and 9 show the energy of the system as function of time for $0 \leq t/t_0 \leq 150$, and for $0 \leq t/t_0 \leq 400$, respectively.

As seen in these graphs, the symmetric configuration (Fig. 2) merges quickly into one soliton and as time increases, it eventually approaches the equilibrium solution. On the other hand, the two blobs do not merge in the antisymmetric case (Fig. 8). This is a direct consequence of the fact that the initial configuration has a node at $\theta = 0$. Because of the symmetry between θ and $-\theta$, $\Psi(\theta = 0, t)$ must be zero for all times $t > 0$. As a result, the two blobs never merge as a simple consequence of parity conservation. The parity operator commutes with the Hamiltonian, and parity is therefore a conserved quantity. Only numerical errors can eventually lead to a single-soliton profile (with lower energy). That this does not happen provides a check on the accuracy of our numerics.

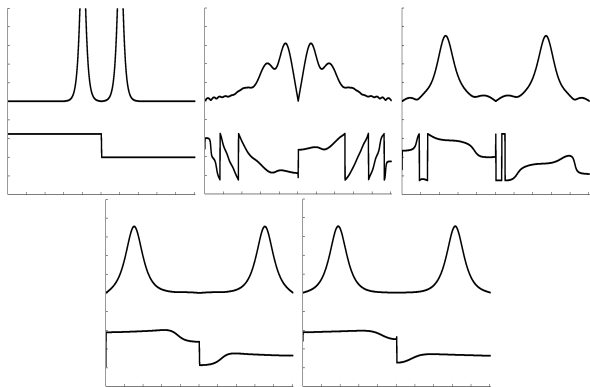


FIG. 8: Snapshots of $|\Psi(\theta, t)|$ (higher curve in each panel) and of $\phi(\theta, t)$ (lower curve in each panel) of the order parameter $\Psi = |\Psi(\theta, t)|e^{i\phi(\theta, t)}$, for the antisymmetric initial configuration, $\alpha = -1$, for $t/t_0 = 0, 10, 100, 300$, and 400 . The axes are the same as in Fig. 1. In all the above graphs there is no external potential, $V = 0$.

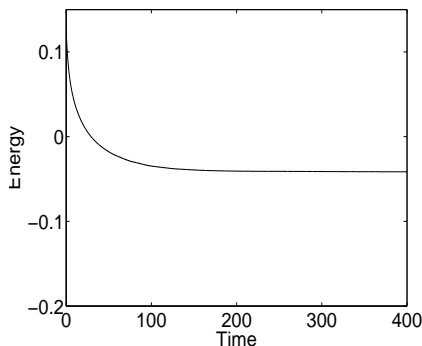


FIG. 9: The energy of the system in units of $E_0 = \hbar^2/(2MR^2)$, versus time for $0 \leq t/t_0 \leq 400$ corresponding to Fig. 8.

IV. EFFECT OF THE RANDOM POTENTIAL ON THE TIME EVOLUTION

Using Figs. 2 and 8 as “reference plots”, we may now examine the effect of a weak, symmetry breaking random potential $V(\theta)$. This potential is chosen to consist of ten steps of equal widths with a height that is a (uniformly distributed) random number and varies between 0 and 0.01. Figure 14 shows the specific random potential chosen. In this case we start with perfectly symmetric/antisymmetric configurations, $\alpha = \pm 1$.

The time evolution of the symmetric configuration shown in Figs. 4 and 5 is almost identical with that of Figs. 2 and 3, i.e., the case considered in the previous section with $V = 0$. The two blobs merge rather rapidly. The antisymmetric case shown in Figs. 10 and 11 is of greater interest. Here, after a relatively short time, the system passes through a “quasi-equilibrium” configuration, seen as the plateau in the plot of energy versus time in Fig. 11. During this time interval, there are two localized blobs. However, parity is no longer a conserved

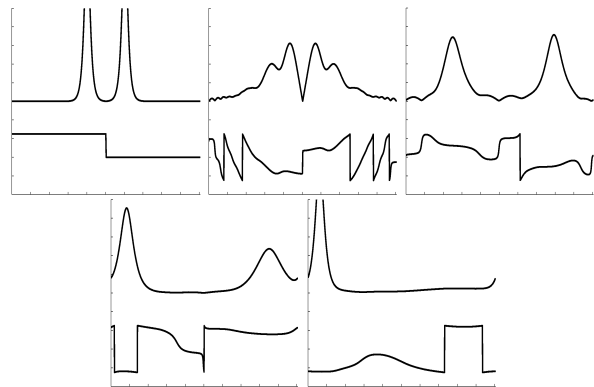


FIG. 10: Snapshots of $|\Psi(\theta, t)|$ (higher curve in each panel) and of $\phi(\theta, t)$ (lower curve in each panel) of the order parameter $\Psi = |\Psi(\theta, t)|e^{i\phi(\theta, t)}$, for the antisymmetric initial condition, for $t/t_0 = 0, 10, 100, 300$, and 400 , for a weak random potential (shown in Fig. 14), with an antisymmetric initial condition, $\alpha = -1$. The axes are the same as in Fig. 1.

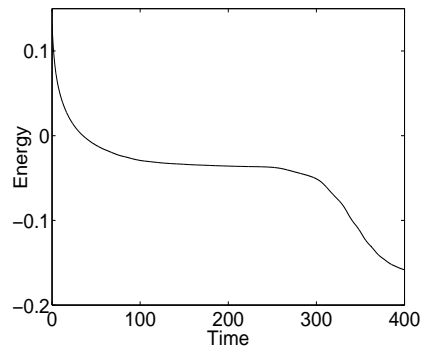


FIG. 11: The energy of the system in units of $E_0 = \hbar^2/(2MR^2)$, versus time for $0 \leq t/t_0 \leq 400$ corresponding to Fig. 10.

quantity in this case. There is no symmetry in the system to preserve the node that was built into the initial conditions. As a result, the two blobs eventually merge into one in contrast to the results of Fig. 8. In other words, the apparent repulsion of the two solitary waves is not present at sufficiently large t .

V. EFFECT OF SLIGHT ASYMMETRIES IN THE INITIAL CONFIGURATION

In another set of runs, we set the random potential to zero and select slightly asymmetric initial configuration, with $\alpha = \pm 1.01$. Our initial condition is thus not a parity eigenstate and our calculations show that again the two initially distinct blobs merge after a characteristic timescale. The qualitative features of this calculation are the same as in the case of a random potential described in the previous section.

In the case of an almost symmetric initial configuration, $\alpha = 1.01$ shown in Fig. 6, the two separate blobs

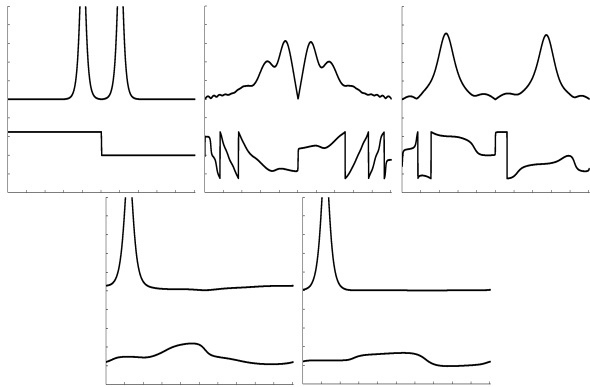


FIG. 12: Snapshots of $|\Psi(\theta, t)|$ (higher curve in each panel) and of $\phi(\theta, t)$ (lower curve in each panel) of the order parameter $\Psi = |\Psi(\theta, t)|e^{i\phi(\theta, t)}$, for the almost antisymmetric initial condition, $\alpha = -1.01$, for $t/t_0 = 0, 10, 100, 300,$ and 400 . The axes are the same as in Fig. 1. In all the above graphs there is no external potential, $V = 0$.

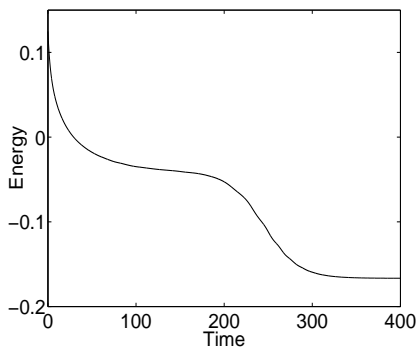


FIG. 13: The energy of the system in units of $E_0 = \hbar^2/(2MR^2)$, versus time for $0 \leq t/t_0 \leq 400$ corresponding to Fig. 12.

merge rapidly, very much as in Figs. 2 and 4. On the other hand, the almost antisymmetric case, $\alpha = -1.01$ shown in Figs. 12 and 13, shows a plateau in the energy and a period of “quasi-equilibrium” during which the two blobs have relatively well-determined shape and location. Eventually, however, the two blobs merge again into a single solitary wave, much as in Fig. 10 but unlike Fig. 8.

VI. DISCUSSION AND CONCLUSIONS

According to the results of our study, the observed repulsion between bright solitary waves in the experiment of Ref. [5] implies that the conservation laws were not substantially violated during the time interval investigated. More precisely, it suggests that deviations from axial symmetry in the trapping potential must have been small, the initial configuration was very close to a (neg-

ative) parity eigenstate, and that dissipation must have been weak.

It is instructive to estimate the timescale, t_0 , for our

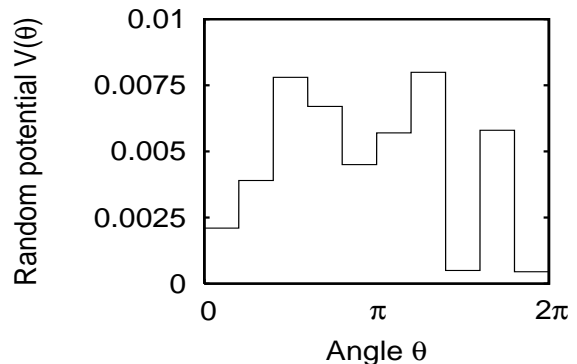


FIG. 14: The random potential in units of $E_0 = \hbar^2/(2MR^2)$ as function of the angle θ that is used in the specific calculations shown in Figs. 4 and 10.

study. If one considers a value of R equal to the longitudinal size of an elongated trap, $R \sim 0.1$ mm, then $t_0 \sim 10$ sec, which is a rather long timescale for these experiments. Therefore, it seems likely that the characteristic timescale over which the experiment of Ref. [5] was performed was significantly smaller than the timescale required to see the separate blobs merge. Higher temperatures would enhance the dissipation in the gas and would decrease the characteristic time that is required for the blobs to merge. To the extent that the deviations from axial symmetry in the trapping potential and the antisymmetry in the initial configuration considered here are representative of the actual experimental situation, our results support the explanation offered in Ref. [7]. Direct experimental determinations of these quantities and of the strength of dissipation would thus be welcome. It would also be of interest to investigate the long time stability (or instability) of the configurations observed in Ref. [5].

The questions examined here may also have important consequences on possible technological applications. For example, propagation of such solitary waves in waveguides may serve as signals that transfer energy or information. Therefore, understanding and possibly controlling the way that such waves interact with each other may be important. Recent experimental progress in building quasi-one-dimensional and toroidal traps should make such experiments easier to perform and worth investigating.

Acknowledgments

We thank Magnus Ögren for useful discussions.

-
- [1] A. D. Jackson, G. M. Kavoulakis, and C. J. Pethick, *Phys. Rev. A* **58**, 2417 (1998).
- [2] L. Salasnich, A. Parola, and L. Reatto, *Phys. Rev. A* **65**, 043614 (2002).
- [3] S. Burger, K. Bongs, S. Dettmer, W. Ertmer, K. Sengstock, A. Sanpera, G. V. Shlyapnikov, and M. Lewenstein, *Phys. Rev. Lett.* **83**, 5198 (1999).
- [4] J. Denschlag, J. E. Simsarian, D. L. Feder, Charles W. Clark, L. A. Collins, J. Cubizolles, L. Deng, E. W. Hagley, K. Helmerson, W. P. Reinhardt, S. L. Rolston, B. I. Schneider, and W. D. Phillips, *Science* **287**, 97 (2000).
- [5] K. E. Strecker, G. B. Partridge, A. G. Truscott, and R. G. Hulet, *Nature* **417**, 150 (2002).
- [6] L. Khaykovich, F. Schreck, G. Ferrari, T. Bourdel, J. Cubizolles, L. D. Carr, Y. Castin, and C. Salomon, *Science* **296**, 1290 (2002).
- [7] U. Al Khawaja, H. T. C. Stoof, R. G. Hulet, K. E. Strecker, and G. B. Partridge *Phys. Rev. Lett.* **89**, 200404 (2002).
- [8] L. D. Carr and Y. Castin, *Phys. Rev. A* **66**, 063602 (2002).
- [9] L. Salasnich, A. Parola, and L. Reatto, *Phys. Rev. A*, **66**, 043603 (2002).
- [10] J. P. Gordon, *Optics Lett.* **8**, 596 (1983).
- [11] L. D. Carr, C. W. Clark, and W. P. Reinhardt, *Phys. Rev. A* **62**, 063611 (2000).
- [12] S. Gupta, K. W. Murch, K. L. Moore, T. P. Purdy, and D. M. Stamper-Kurn, *Phys. Rev. Lett.* **95**, 143201 (2005).
- [13] C. Ryu, M. F. Andersen, P. Clade, Vasant Natarajan, K. Helmerson, W. D. Phillips, *Phys. Rev. Lett.* **99**, 260401 (2007).
- [14] Rina Kanamoto, Hiroki Saito, and Masahito Ueda, *Phys. Rev. A* **68**, 043619 (2003).
- [15] G. M. Kavoulakis, *Phys. Rev. A* **67**, 011601(R) (2003).